**Proceedings of the ASME 2010 3rd Joint US-European Fluids Engineering Summer Meeting and
8th International Conference on Nanochannels, Microchannels, and Minichannels
FEDSM-ICNMM2010
August 1-5, 2010, Montreal, Canada**

FEDSM-ICNMM2010-30379

A FLUID DYNAMICS STUDY OF A MODIFIED LOW-REYNOLDS-NUMBER FLAPPING MOTION

M. R. Amiralaei
Department of Aerospace Engineering, Ryerson University
Toronto, ON, Canada, M5B 2K3
mamirala@ryerson.ca

H. Alighanbari
Department of Aerospace Engineering, Ryerson University
Toronto, ON, Canada, M5B 2K3
halighan@ryerson.ca

S. M. Hashemi
Department of Aerospace Engineering, Ryerson University
Toronto, ON, Canada, M5B 2K3
smhashem@ryerson.ca

ABSTRACT

The objective of the present study is to investigate the low Reynolds number (LRN) fluid dynamics of an elliptic airfoil performing a novel figure-eight-like motion. To this mean, the influence of phase angle between the pitching and translational (heaving and lagging) motions and the amplitude of translational motions on the fluid flow is simulated. Navier-Stokes (NS) equations with Finite Volume Method (FVM) are used and the instantaneous force coefficients and the fluid dynamics performance, as well as the corresponding vortical structures are analyzed. Both the phase angle and the amplitudes of horizontal and vertical motions are of great importance to the fluid dynamic characteristics of the model as they are shown to change the peaks of the fluid forces, fluid dynamic performance, and the vortical patterns around the model.

INTRODUCTION

Forced and flow-induced oscillations are highly prevalent in a wide range of fluid engineering applications. These unsteady conditions could be useful when assisting in the generation of the fluid forces such as wing flapping, or be destructive when becoming the undesired oscillations such as wing flutter. Flapping motions are the most common means of force generation in micro aerial vehicles and swimming robots. The physical characteristics and the fluid phenomena of such motions strongly depend on the governing flow and system parameters. LRN flapping flows are mostly accompanied with non-linear vortex dynamics, such as dynamic stall [1], rotational movement and fast pitch-up [2], wake-capturing [3], and Weis-Fogh's clap and fling mechanism [4].

Fluid dynamicists have recently shown a growing interest in LRN flapping motions owing to their increasing applications. This has helped to illuminate the details of the respective fluid physics. Some parametric studies have also been performed to identify the important parameters and their effects on the fluid dynamic performance of the relevant applications. Yet, more studies are needed to obtain better insight into the LRN flapping flows.

Studies can be conducted using analytical, experimental and computational methods. Analytical means are extremely simplified solutions with restricted applicability, and as was shown by Ellington [5], the aerodynamic forces predicted by classical analytical methods are inaccurate and unreliable for flapping motions.

Experimental techniques are the most reliable methods for investigating the flow around a flapping wing, but are rather expensive. Experimental studies by Freymuth [6], Issac et al. [7], and Nagai et al. [8] showed the importance of the non-linear vortex dynamics and helped in obtaining a better idea about the effective governing parameters in the force generation.

CFD is also widely used in LRN flapping studies. Bos et al. [9] simulated different flapping kinematics and compared their aerodynamic performance. Kinsey and Dumas [10] investigated the flow field of a flapping airfoil numerically and found that system parameters such as plunging amplitude and frequency are the most influential ones on the fluid flow. Tang et al. [11] simulated the flow field of a hovering elliptic airfoil and investigated the effects of Reynolds number (Re), reduced frequency, and flapping kinematics on the aerodynamics. Lee et al. [12] investigated the role of leading and trailing edge vortices (LEV and TEV) on the aerodynamic force generation and showed that LEV affects thrust generation in addition to its effect on increasing the lift during plunging motion. The 2D figure-eight-like motion simulations by Lee et al. [13] showed that the lift is mainly produced during downstroke, while the thrust is mostly achieved at the end of the upstroke. They attributed the generated thrust to the vortex pairing which is different from the conventional inverse Karman vortex street found in sinusoidal flapping motions.

The objective of the present study is to investigate the fluid dynamics of a flapping airfoil in LRN regime. The flow field of the model performing a modified figure-eight-like pattern is simulated, and the effects of the amplitude of translational motions and phase lag/lead between the pitching and translational motions on the fluid dynamic characteristics of the model are explored. CFD is the utilized solution method and the governing equations are the 2D NS equations discretized based on FVM. The computations are carried out in OpenFOAM [14].

NOMENCLATURE

c	=	airfoil chord-length
C_d	=	drag coefficient
C_l	=	lift coefficient
C_m	=	pitching moment coefficient
T	=	period of oscillation
τ	=	non-dimensional time (t/T)
LEV/TEV	=	leading/trailing edge vortex

NUMERICAL SIMULATION METHOD

The non-dimensional form of NS equations, governing the fluid flow of a 2D airfoil in LRN flows, is:

$$\begin{aligned}
&\frac{\partial u}{\partial x}+\frac{\partial v}{\partial y}=0\\
&\frac{\partial u}{\partial t}+u\frac{\partial u}{\partial x}+v\frac{\partial u}{\partial y}=-\frac{\partial p}{\partial x}+\frac{1}{\mathrm{Re}}\left(\frac{\partial^2 u}{\partial x^2}+\frac{\partial^2 u}{\partial y^2}\right)\\
&\frac{\partial v}{\partial t}+u\frac{\partial v}{\partial x}+v\frac{\partial v}{\partial y}=-\frac{\partial p}{\partial x}+\frac{1}{\mathrm{Re}}\left(\frac{\partial^2 v}{\partial x^2}+\frac{\partial^2 v}{\partial y^2}\right)
\end{aligned} \tag{1}$$

where u, v, and p are the non-dimensional velocity components and pressure, respectively, t is the physical time, and Re stands for the Reynolds number.

O-type mesh is used for the simulations. The far-field boundary with symmetry boundary condition is set to $30c$ from the airfoil, in order to minimize the undesired effect on the airfoil's surrounding flow. The airfoil is set to no-slip boundary condition. The total number of cells was 50×10^3 and 2000 time steps were considered within one excitation period. This choice of grid size and temporal resolution was made after extensive grid and time sensitivity analyses. Fig. 1 shows the schematic of the airfoil, the computational domain, and the investigated flapping kinematics in the present simulations.

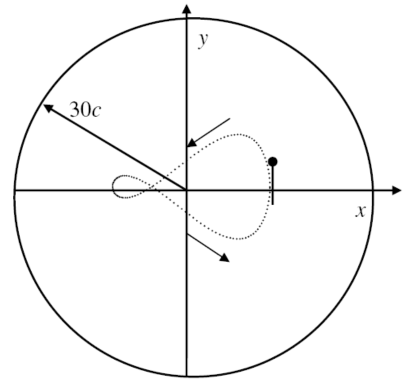

Fig. 1: Computational domain and the kinematics pattern

The fluid dynamics of an ellipse with 2% thickness is investigated based on FVM and NS equations. The computations are based on a second order central differencing scheme for convective and diffusive terms and a second order Euler implicit scheme for temporal discretization. The resulting linear system of equations is treated with Preconditioned Conjugate Gradient (PCG) solvers, and the Semi-Implicit Method for Pressure Linked Equations (SIMPLE) algorithm is used for the pressure-velocity coupling. The computations are carried out in OpenFOAM [14]. The equation of motion in a simplified form is:

$$\begin{aligned}
&x(t)=R\cos(2\pi ft)\\
&y(t)=d\sin(2\pi ft)+R\sin(2\pi ft)\cos(2\pi ft)\\
&\theta(t)=\theta_0-\overline{\theta}\sin(2\pi ft+\varphi)
\end{aligned} \tag{2}$$

where $x(t)$ and $y(t)$ are the horizontal and vertical position vectors of the airfoil mid-chord, respectively, $\theta(t)$ is the instantaneous angle of attack, d and R are the amplitudes of plunging (vertical) and lagging (horizontal) motions, respectively, $\overline{\theta}$ is the amplitude of pitching oscillations, f stands for the frequency of oscillation, θ_0 is the mean angle of attack, and φ is the phase lead/lag between rotational and translational motions. Figure 1 shows the figure-eight pattern obtained from Equations 2.

EVALUATION OF THE RESUTLS

In order to obtain results which are independent of the grid and time step size, several cases are examined.

Four mesh sizes of 12.5, 25, 50, and 100 ($\times10^3$) with 2000 time steps in each flapping period were first considered. According to the results, the mesh with 50×10^3 with 2000 time steps is considered reasonably refined to yield accurate solutions. After obtaining a grid independent solution, the temporal resolution was changed for 500, 1000, 2000, and 4000 time steps in each period having 50×10^3 number of cells. The results show that 2000 time steps are enough for the temporal independent solution. Hence, the mesh with 50×10^3 cells and 2000 time steps is considered to yield accurate solutions.

The validation is based on the cases studied by Wang et al. [16] and Bos et al. [9], where the flapping kinematics is governed by the following equations:

$$x(t) = \frac{A_0}{2}\cos(2\pi f t)$$
$$\alpha(t) = \alpha_0 + \beta \sin(2\pi f t + \phi) \quad (3)$$

with $A_0 = 2.8$, $f = 0.25$, $\alpha_0 = \pi/2$, $\beta = \pi/4$, and $\varphi = 0$.

The simulated C_l and C_d are in reasonably good agreement (less than 5% of difference) with the literature [9, 15]. The discrepancy can be attributed to different schemes used for the discretization of spatial terms in this study (central) and those used in Refs. 9 and 15. It may also be due to the different LE and TE shapes of the ellipse model. Figure 2 shows the comparison between the lift coefficients.

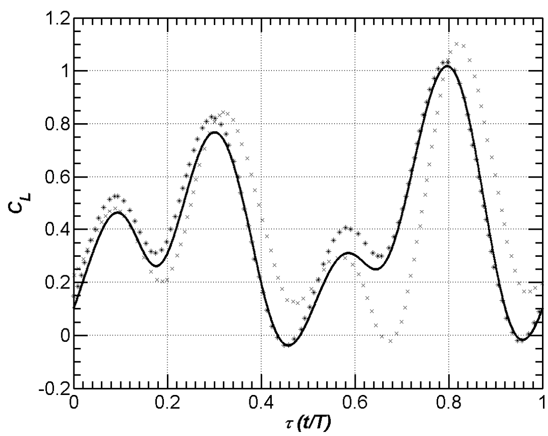

Fig. 2: The comparison between C_l vs τ of the present simulations: (—), Bos et al [9]: (*), and Wang et al [15]: (×) for harmonic flapping of Equations 3, $A_0 = 2.8$, $f = 0.25$, $\alpha_0 = \pi/2$, $\beta = \pi/4$, and $\varphi = 0$

RESULTS AND DISCUSSION

Consider a 2D ellipse with 2% thickness and chord-length c performing the figure-eight motion according to Equations 2. In this analysis, the effect of phase angle (φ) and the amplitudes of translational oscillations (d and R) on the fluid dynamic characteristics of the model is explored. The analysis is performed in terms of C_l, C_d, and $\overline{C}_l/\overline{C}_d$. The generated vortical structures around the airfoil are also studied in detail at the points of interest, i.e. the peaks of C_l.

Effects of phase lag/lead

The effect of phase lag/lead is investigated for φ = -π/6 (delayed), φ = 0 (symmetrical), and φ = π/6 (advanced) rotations. Figure 3 presents C_l versus τ. As can be seen, the primary peak of the lift coefficient, $C_{l,\max}$, decreases from 4.53 to 4.03 when φ is changed from -π/6 (delayed) to 0 (symmetrical) rotations. Similarly, the primary $C_{l,\max}$ decreases from 4.03 to 1.89 when φ is changed from 0 (symmetrical) to π/6 (advanced) rotations. However, the percentage of decrease from symmetrical to advanced cases is much higher than that of the delayed to symmetrical rotations.

On the other hand, φ has an inverse effect on the secondary peak lift coefficient (Fig. 3), i.e. the secondary $C_{l,\max}$ increases when the phase angle is changed from delayed to symmetric and from symmetric to advanced rotations. Moreover, the percentage of increase of the secondary $C_{l,\max}$ is more than that of the primary peak, which means that φ has a stronger impact on the secondary $C_{l,\max}$. The vorticity plots around the airfoil are shown in Figs. 4 and 5, which show the vortical patterns when the primary and secondary $C_{l,\max}$, respectively, are obtained. As can be seen in Fig. 4, both LEV/TEV turn out to be closer to the airfoil surface when increasing φ from -π/6 to 0 and from 0 to π/6. The LEV/TEV interaction is also decreased when increasing φ. This behavior could be related to the decrease of the primary $C_{l,\max}$ previously seen in figure 3. However, the vortical structures around the airfoil show an inverse behavior at the secondary $C_{l,\max}$ (Fig. 5). It means that LEV/TEV are more convected into the downstream wake of the airfoil which could be the reason for the increasing trend of the variation of the secondary $C_{l,\max}$. It should be mentioned that the vortices in Figs. 4 and 5 are attached to the airfoil surface and separation does not occur.

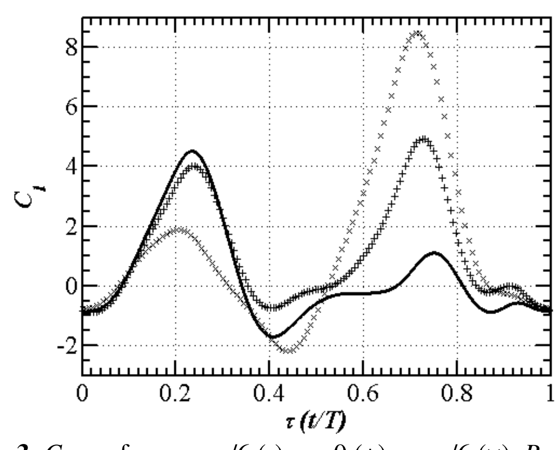

Fig. 3: C_l vs τ for: φ = -π/6 (-),φ = 0 (+),φ = π/6 (×), R = 1.4, d = 0.7, f = 0.25, $\overline{\theta}$ = π/4, θ_0 = π/2, and Re = 75

a) φ = -π/6 *b*) φ = 0 *c*) φ = π/6

Fig. 4: Vorticity contours at the primary $C_{l,\max}$; R = 1.4, d = 0.7, f = 0.25, $\bar{\theta}$ = π/4, θ_0 = π/2, and Re = 75

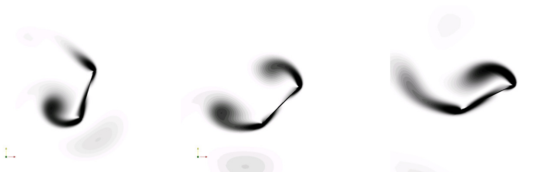

a) φ = -π/6 *b*) φ = 0 *c*) φ = π/6

Fig. 5: Vorticity contours at the secondary $C_{l,\max}$; R = 1.4, d = 0.7, f = 0.25, $\bar{\theta}$ = π/4, θ_0 = π/2, and Re = 75

Figure 6 shows C_d versus τ for φ = -π/6, φ = 0, and φ = π/6. As can be seen, increasing φ from -π/6 to 0 and from 0 to π/6 increases the first peak of drag coefficient ($C_{d,\max}$), but it has an inverse effect on the second peak. Moreover, increasing φ from 0 to π/6 induces another peak in C_d around τ=0.4 (Fig. 6). As shown in Fig. 7, the phase angle has similar effects on pitching moment coefficient (C_m) as those on C_d.

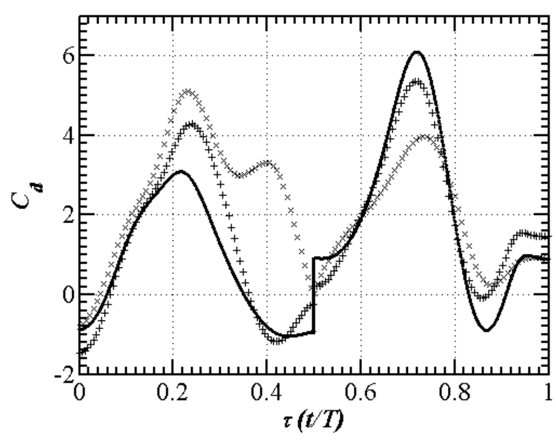

Fig. 6: C_d vs τ for: φ = -π/6 (-),φ = 0 (+),φ = π/6 (×), R = 1.4, d = 0.7, f = 0.25, $\bar{\theta}$ = π/4, θ_0 = π/2, and Re = 75

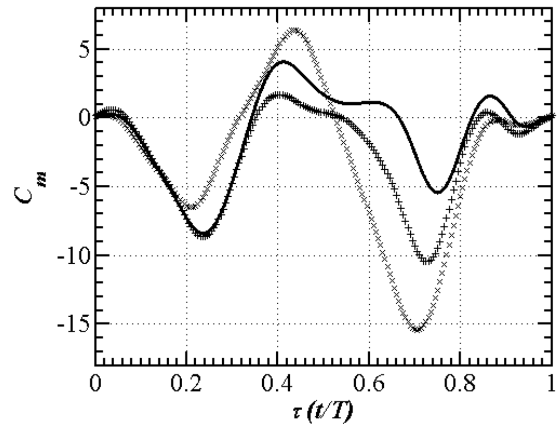

Fig. 7: C_m vs τ for: φ = -π/6 (-),φ = 0 (+),φ = π/6 (×), R = 1.4, d = 0.7, f = 0.25, $\bar{\theta}$ = π/4, θ_0 = π/2, and Re = 75

The fluid dynamic performance ($\overline{C}_l/\overline{C}_d$) of the model for the considered phase angles are presented in table 1. The table shows that the symmetric rotation case has the highest and the delayed rotation case has the lowest performance.

Table 1: Aerodynamic performance for the conducted simulations; R = 1.4, f = 0.25, $\bar{\theta}$ = π/4, θ_0 = π/2, and Re = 75

d	φ	$\overline{C}_l/\overline{C}_d$
0.7	0	0.705
0.7	-π/6	0.238
0.7	π/6	0.614
0.4	0	0.701
1	0	0.681

Effects of translational amplitude of oscillation

The effect of the amplitudes of oscillations is investigated using d = 0.4, 0.7, and 1 and R = 1 and 1.4. Increasing d has the same effect on the first and second $C_{l,\max}$, Fig. 8. Increasing d from 0.4 to 0.7 increases $C_{l,\max}$. However, $C_{l,\max}$ decreases when d is increased from 0.7 to 1. Increasing d has similar effects on C_d and $C_{d,\max}$ as shown in figure 9. Figures 10 and 11 show the instantaneous lift and drag coefficients, respectively, for R = 1 and 1.4, and present the effect of increasing the amplitude of the lagging (horizontal) motion. The figures show that increasing R decreases both $C_{l,\max}$ and $C_{d,\max}$, and R has stronger effect on the fluid dynamics forces than d.

The fluid dynamic performance ($\overline{C}_l/\overline{C}_d$) of the model for the considered amplitudes of plunging (vertical) motion is presented in table 1, which show that d does not have any noticeable effect on the performance.

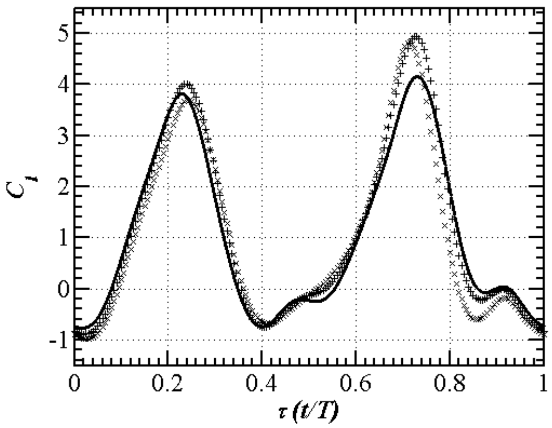

Fig. 8: C_l vs τ for: d = 0.4 (-), d = 0.7 (+), d = 1 (×), R = 1.4, f = 0.25, $\bar{\theta}$ = π/4, θ_0 = π/2, φ = 0, Re = 75

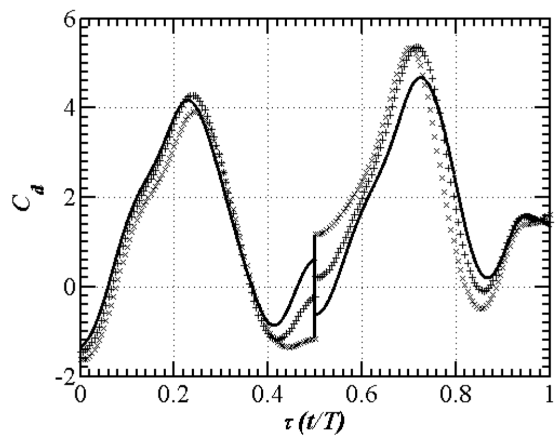

Fig. 9: C_d vs τ for: d = 0.4 (-),d = 0.7 (+),d = 1 (×), R = 1.4, f = 0.25, $\bar{\theta}$ = π/4, θ_0 = π/2, φ = 0, Re = 75

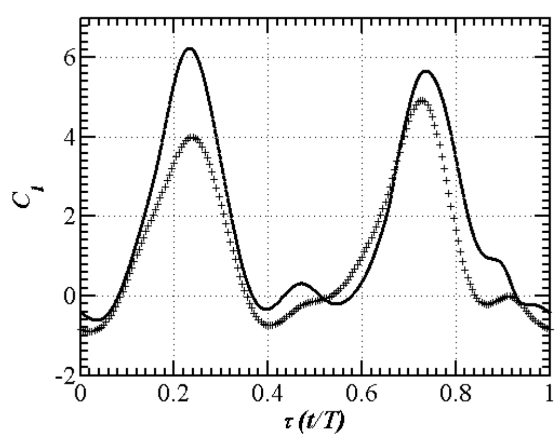

Fig. 10: C_l vs τ for: R = 1 (-), R = 1.4 (+), d = 0.7, f = 0.25, $\bar{\theta}$ = π/4, θ_0 = π/2, φ = 0, Re = 75

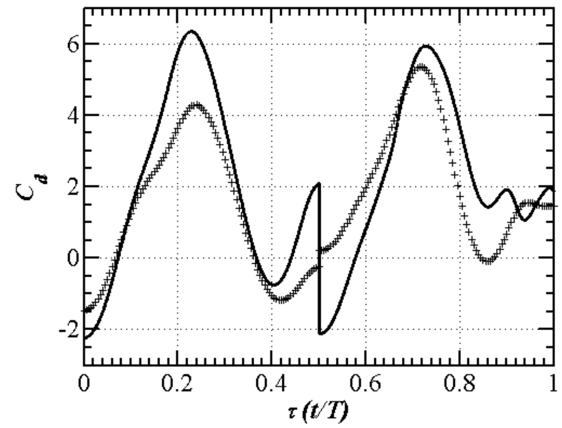

Fig. 11: C_d vs τ for: R = 1 (-), R = 1.4 (+), d = 0.7, f = 0.25, $\bar{\theta}$ = π/4, θ_0 = π/2, φ = 0, Re = 75

CONCLUSION

Numerical study of flow around an elliptic airfoil under a novel flapping kinematics is carried out, and the effects of the phase angle and the amplitudes of translational motions are investigated in laminar flow range. Navier-Stokes equations and finite volume approach are used and lift and drag coefficients are analyzed as well as the fluid dynamics performance. The generated vortical patterns around the model are also explored. Both phase angle and amplitudes of oscillations are found to have great influence on the fluid flow force generation and on the LEV/TEV behavior. They change the magnitude of the fluid forces, specifically their peak values. Phase angle affects the fluid dynamic performance, while the influence of the amplitudes of oscillations is negligible compared to the phase angle effect. When changing the phase angle, the vortical patterns around the model are found to be different at the peaks of fluid forces. This difference is the major reason for the different magnitude of the peaks observed in the simulation results.

REFERENCES

[1] Ellington, C. P., Van den Berg, C., Willmott, A. P., and Thomas, A. L. R., “Leading Edge Vortices in Insect Flight, ” Nature(London), Vol. 384, No. 6610, 1996, pp. 626-630.

[2] Freymuth, P., “Propulsive Vortical Signatures of Plunging and Pitching Airfoils,” AIAA Paper 88-0323, 1988.

[3] Dickinson, M. H., Lehmann, F. O., and Sane S. P., “Wing Rotation and the Aerodynamic Basis of Insect Flight,” Science, Vol. 284, No. 5422, 1999, pp. 1954-1960.

[4] Weis-Fogh, T., “Quick Estimates of Flight Fitness in Hovering Animals, Including Novel Mechanisms for Lift

Production," Journal of Experimental Biology, Vol. 59, No. 1, 1973, pp. 169-230.

[5] Ellington, C. P., "The Aerodynamics of Hovering Insect Flight, the Quasi-Steady Analysis," Philosophical Transactions of the Royal Society of London, Series B: Biological Sciences, Vol. 305, No. 1122, 1984, pp. 1-15.

[6] Freymuth, P., "Thrust Generation by an Airfoil in Hover Modes," *Experiments in Fluids*, Vol. 9, 1990, pp. 17-24.

[7] Issac, K., M., Rolwes, J., and Colloza, A., "Aerodynamics of a Flapping and Pitching Wing Using Simulations and Experiments," *AIAA Journal*, Vol. 46, No. 6, 2008, pp. 1505-1515.

[8] Nagai, H., Isogai, K., Fujimoto, T., and Hayase, T., "Experimental and Numerical Study of Forward Flight Aerodynamics of Insect Flapping Wing," *AIAA Journal*, Vol. 47, No. 3, 2009, pp. 730-742.

[9] Bos, F., M., Lentink, D., Van Oudheusden, B., W., and Bijl, "Influence of Wing Kinematics on Aerodynamic Performance in Hovering Insect Flight," *J. Fluid Mech.*, Vol. 594, 2008, pp. 341-368.

[10] Kinsey, T., and Dumas, G., "Parametric Study of an Oscillating Airfoil in a Power-Extraction Regime," *AIAA Journal*, Vol. 46, No. 6, 2008, pp. 1318-1330.

[11] Tang, J., Viieru, D., Shyy, W., "Effects of Reynolds Number and Flapping Kinematics on Hovering Aerodynamics," *AIAA Journal*, Vol. 46, No. 4, 2008, pp. 967-976.

[12] Lee, J., S., Kim, J., H., and Kim, C., "Design of Flapping Airfoil for Optimal Aerodynamic Performance in Low-Reynolds Number Flows," *AIAA Journal*, Vol. 44, No. 9, 2006, pp. 1960-1972.

[13] Lee, J., S., Kim, J., H., and Kim, C., "Numerical Study on the Unsteady-Force-Generation Mechanism of Insect Flapping Motion," *AIAA Journal*, Vol. 46, No. 7, 2008, pp. 1835-1848.

[14] OpenFOAM, the Open Source CFD Toolbox, User Guide, version 1.4.1, August 2007.

[15] Wang, Z. J., Birch, J. M., and Dickinson, M. H., "Unsteady Forces and Flows in Low Reynolds Number Hovering Flight: Two-Dimensional Computations vs Robotic Wing Experiments," The Journal of Experimental Biology, Vol. 207, 2004, pp. 449-460.